

# Laser Transmission Spectroscopy Based on Tunable-Gain Dual-Channel Dual-Phase LIA for Biological Nanoparticles Characterization

Angelo Sarra, Guido Di Patrizio Stanchieri , Andrea De Marcellis , *Member, IEEE*, Federico Bordi, Paolo Postorino, and Elia Palange 

**Abstract**—Size and absolute concentration of suspensions of nanoparticles are important information for the study and development of new materials and products in different industrial applications spanning from biotechnology and pharmaceuticals to food preparation and conservation. Laser Transmission Spectroscopy (LTS) is the only methodology able to measure nanoparticle size and concentration by performing a single measurement. In this paper we report on a new variable gain calibration procedure for LTS-based instruments allowing to decrease of an order of magnitude the experimental indetermination of the particle size respect to the conventional LTS based on the double ratio technique. The variable gain calibration procedure makes use of a specifically designed tunable-gain, dual-channel, dual-phase Lock-In Amplifier (LIA) whose input voltage signals are those ones generated by two Si photodiodes that measure the laser beam intensities passing through the sample containing the nanoparticles and a reference optical path. The LTS variable gain calibration procedure has been validated by firstly using a suspension of NIST standard polystyrene nanoparticles even 36 hours after the calibration procedure was accomplished. The paper reports in detail the LIA implementation describing the design methodologies and the electronic circuits. As a case example of the characterization of biological nanostructures, we demonstrate that a single LTS measurement allowed to determine size density distribution of a population of extracellular vesicles extracted from orange juice (25 nm in size) with the presence of their aggregates having a size of 340 nm and a concentration smaller than 3 orders of magnitude.

**Index Terms**—Bacteria detection, biological nanoparticles characterization, extracellular vesicle size and concentration measurement, laser transmission spectroscopy, lock-in amplifier.

## I. INTRODUCTION

**I**N THE last decades, the study of nanoparticle suspensions has become fundamental to different fields, from medical biotechnologies, to pharmaceuticals, to food industry and, in general, for the development and characterization of new materials [1]–[5].

At present, one of the top challenges in microbiology is the characterization of the membrane vesicles produced and released by Eukarya and Bacteria for inter-species and inter-kingdom interactions [6]–[8]. Actually, practically every cell type in an organism, including for example dendritic cells, lymphocytes and cancer cells, actively release small (from 30 to 100 nm in diameter) membrane vesicles, referred as exosomes, into biofluids (i.e., plasma/serum, urine, cerebrospinal fluid and saliva). These vesicles are powerful cell-to-cell messengers containing nucleic acids, proteins and other small molecules, and begin to be exploited as innovative and effective biomarkers for the diagnosis of many different diseases (i.e., different type of cancer, kidneys diseases, gastrointestinal disorders, etc.) [9]–[11].

Also, in food preservation, where a great research effort has been devoted to the detection of bacteria in the fruit juice, which is often associated with loss of flavor and bitter taste [12], exosomes could represent a powerful diagnostic tool for detecting bacterial contamination. A further hot research topic in the food industry, is the design of “functional food”. In particular, several benefits for human health are associated with the consumption of probiotic bacteria, also through the assumption of supplemented fruit juices [13], [14]. Also in this case, the extracellular vesicles are credited to play a central role. For example, it has been shown that nanovesicles secreted both by the bacteria and by the edible plants may have implications for human health, with anti-inflammatory properties in inflammatory bowel diseases and inhibitory properties in cancer cell proliferation [15]–[17]. Moreover, although nanovesicles play a role of primary interest in all these fields, their extraction, isolation, characterization and, above all their quantification, still represent an extremely

Manuscript received October 5, 2020; revised December 31, 2020; accepted February 13, 2021. Date of publication February 19, 2021; date of current version March 30, 2021. (*Corresponding author: Andrea De Marcellis.*)

Angelo Sarra is with the Liquid Group, Department of Science, University of Roma Tre, Rome 00146, Italy, and also with the High Pressure Spectroscopy (HPS) Group, Department of Physics, Sapienza University, 00185 Rome, Italy (e-mail: angelo.sarra@uniroma3.it).

Guido Di Patrizio Stanchieri, Andrea De Marcellis, and Elia Palange are with the Electronic and Photonic Integrated Circuits and Systems (EPICS) Laboratory, Department of Industrial and Information Engineering and Economics, University of L'Aquila, 67100 L'Aquila, Italy (e-mail: guido.dipatriziostanchieri@graduate.univaq.it; andrea.demarcellis@univaq.it; elia.palange@univaq.it).

Federico Bordi is with the Physics of Bio-Assemblies (PhoBiA) Group, Department of Physics, Sapienza University, 00185 Rome, Italy (e-mail: federico.bordi@roma1.infn.it).

Paolo Postorino is with the High Pressure Spectroscopy (HPS) Group, Department of Physics, Sapienza University, 00185 Rome, Italy (e-mail: paolo.postorino@roma1.infn.it).

Color versions of one or more figures in this article are available at <https://doi.org/10.1109/TBCAS.2021.3060569>.

Digital Object Identifier 10.1109/TBCAS.2021.3060569

difficult task to be fulfilled due to their nanometer size and low concentration [18].

In this scenario, relatively simple techniques allowing to recognize, quantify, and characterize suspended nanoparticles (and particularly the exosomes) would be really welcome. The Laser Transmission Spectroscopy (LTS) could be the technique of choice to accomplish these goals. LTS is an optical technique that allows to determine the presence of micro- and nano-particles like vesicles and bacteria in fluid suspension in a wide range of sizes and concentrations, with a large applicability in different scientific and technological fields [19]–[22]. LTS technique measures the optical transmission coefficient of any suspension of particles as a function of the wavelength of a probing laser beam passing through the sample. By using the Beer-Lambert's law, the Mie and/or Bohren-Huffman scattering theory and the Tikhonov inversion methods, it is possible to calculate the particle density distribution as a function of their size. Differently from the traditional Dynamic Light Scattering (DLS) technique [23], LTS allows not only to determine the actual size of the particles in suspension (remember that DLS measures an equivalent hydrodynamic radius, i.e., the radius of a sphere with the same diffusion coefficient as the particles in suspension) but also to evaluate their absolute concentration. Moreover, LTS technique can also furnish some useful information on the shape and structure of the particles (for example the presence of coatings or shells surrounding the particles). This result is important for the fast characterization of samples in biophysics and biomedicine allowing also to foresee the introduction of new therapeutic and diagnostic techniques [17], [24].

In order to measure the wavelength dependent transmission coefficient, an LTS apparatus makes use of a tunable laser whose output beam is properly divided in two beams of equal intensity that propagate along two different optical paths: one containing the sample under study (the sample channel) and the other one containing the reference sample (the reference channel). In general, for the applications of interest of the present paper, the sample is an aqueous suspension of biological particles and the reference is simply the aqueous suspending medium. Thus, respect to the beam propagating in the reference channel, that one passing through the sample channel experiences light scattering due to the presence of the particles under study and this decreases the intensity, in particular, of the emerging beam in the forward direction. Independently from this, in real experimental apparatus, intensity variations of the laser beam propagating through the sample and the reference channels can present differences due to the non-identical characteristics of the employed optical and optoelectronic components like mirrors, beam splitters, lenses and photodetectors used to evaluate laser intensity variations in each one of the two channels. This represents an important drawback when measuring small variations of the transmission coefficient of particles with very small sizes and/or low concentrations. To avoid this problem LTS measurements are performed by employing the double ratio paradigm consisting in making two different measurements of the transmission coefficient by interchanging the sample and the reference holders in the two optical paths to cancel out any

physical and optical differences between the two channels [19]. The intensities of the two transmitted laser beams are detected by two photodiodes whose generated voltage signals become the sample and reference input signals of an optoelectronic detection apparatus based on the phase-sensitive synchronous demodulation technique carried out by a Lock-In Amplifier (LIA) used to maximize the Signal-to-Noise Ratio (SNR) in presence of very noisy conditions [25]–[39]. However, the double ratio procedure propagates the measurement indeterminacy, increasing the associated final fractional uncertainty on the values of the particle size and concentration. This represents a disadvantage particularly detrimental when measuring low concentrated samples, as it is the case of vesicles and bacteria in many medical and food applications.

This paper reports the development of a new approach to LTS measurements called variable gain calibration procedure, that makes use of an *ad-hoc* designed tunable-gain, dual-channel, dual-phase LIA. The procedure has been validated to determine the size and concentration of a suspension of NIST standard polystyrene nanoparticles by comparing the achieved results with those ones obtained by using the double ratio technique. After this, as case example of biological nanoparticles, we characterized extracellular vesicles extracted from orange juice by centrifugation followed by filtration. We will demonstrate that the electronic solutions and methodologies employed to fabricate the LIA allowed to maximize the LTS apparatus sensitivity and resolution with respect to small variations of the laser intensity passing through the sample channel. With respect to the double-ratio technique, the proposed LTS measurement method makes use of a single calibration procedure to balance the signals coming from the sample and reference channels when in both the channels is present the suspending medium only. This balanced LTS method is performed by suitably varying the gain of the two LIA channels so to achieve the same value of the sample and reference signals for each wavelength of the probing laser beam. The values of the wavelength dependent gains determined by this calibration procedure, are used for the LTS measurement of the particles under study located in the sample channel. We will demonstrate that the LTS measurement performed in this way is capable to decrease of one order of magnitude the experimental indeterminacy on the size of NIST standard polystyrene nanoparticles respect to the double ratio method even 36 hours after the variable gain procedure was accomplished. Moreover, LTS measurements of extracellular vesicle population allowed to determine their size (25 nm) and density distribution as well as the presence of their aggregates (340 nm in size) with a concentration smaller than 3 orders of magnitude. These results demonstrate that the proposed LTS apparatus is a powerful, reliable tool for research in biology and medicine as well as, for food and life science industrial applications.

Finally, this paper extends the preliminary work reported in [40] providing additional theoretical and technical details, improved circuit design and system implementation, a deeper data analysis and further experimental measurements using both standard and biological nanoparticles.

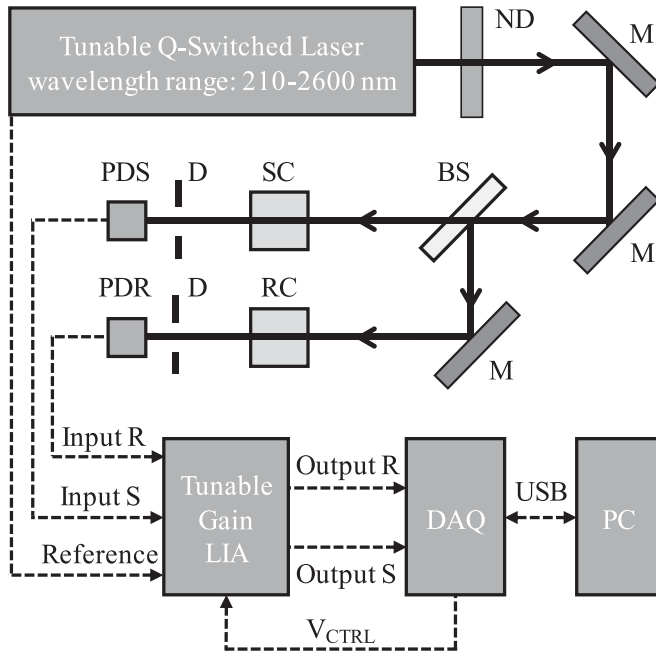


Fig. 1. LTS experimental setup: ND are neutral density filters, M total reflective mirrors, BS a polka-dot 50/50 beam splitter, SC and RC the sample and the reference cuvettes, respectively, D variable diaphragms, PDS and PDR Si photodiodes detecting the laser beam intensity passing through SC and RC, respectively; LIA is the tunable-gain dual-channel, dual-phase Lock-In Amplifier, DAQ is a Data Acquisition board,  $V_{CTRL}$  is the control voltage for the LIA gain tuning and PC a Personal Computer for the data visualization and analysis.

## II. THE LTS MEASUREMENT METHOD AND THE OPTOELECTRONIC DETECTION SYSTEM

### A. The LTS Technique and the Experimental Set-Up

The LTS technique measures the wavelength dependence of the optical transmission coefficient  $T(\lambda, r)$  of a suspension of particles of radius  $r$  in aqueous solution. The particle density distribution as a function of their dimension is obtained by using the Beer-Lambert's relation, by first calculating the extinction coefficient  $\alpha(\lambda, r)$ :

$$\alpha(\lambda, r) = -\frac{\ln[T(\lambda, r)]}{z} \quad (1)$$

where  $z$  is the optical path within the sample. The experimentally determined values of the extinction coefficients for each wavelength are analyzed and inverted by using a square root-based algorithm [41] to return the particle size and concentration. This is achieved through the calculation of the wavelength-size dependent properties of the particles that are identified by the Mie and/or Bohren-Huffman scattering cross-section  $\sigma(\lambda, r)$  [42], [43]. In this regard, for the determination of the particle density distributions reported in the following, we used the Sellmeier equation to evaluate the wavelength dependence of the dielectric permittivity for NIST standard polystyrene nanoparticles and aqueous suspending solutions [44], [45].

The experimental setup implemented for the LTS measurements is shown in Fig. 1. The laser source is a 5 ns Q-Switched Nd:YAG operating at 10 Hz repetition rate (NT342B Ekspla -

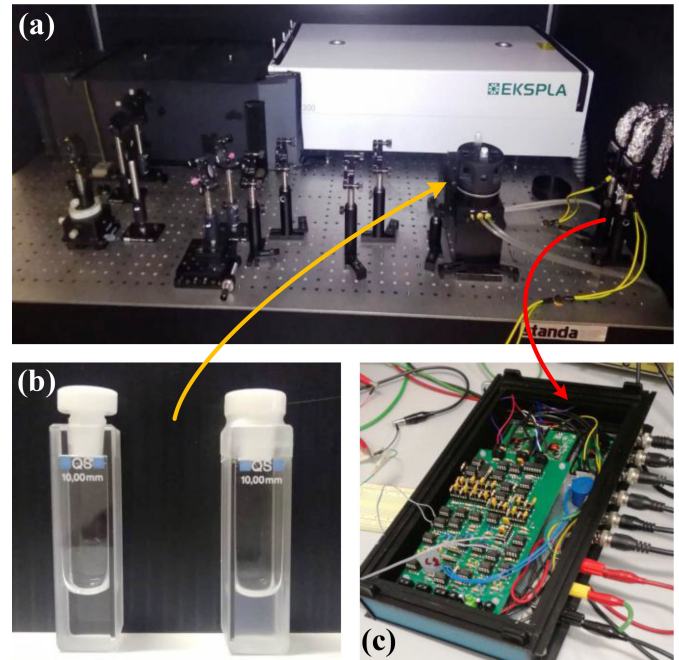


Fig. 2. Panel (a): a photograph of the LTS experimental apparatus; Panel (b): the 1 cm length quartz cuvettes used in the sample and reference optical channels; Panel (c) a photograph of the fabricated LIA.

Vilnius - LT). The laser tunability in the wavelength range 210-2600 nm is achieved by employing an optical parametric amplifier and second and third harmonic generation crystals. The laser beam is aligned parallel to the surface of an optical table by operating on a couple of fully reflecting mirrors located into two-adjuster kinematic mirror mounts. The beam intensity is suitably attenuated by a set of neutral density filters to avoid sample damage.

A wideband polka-dot 50/50 beam splitter (Polka-Dot Beam-splitter by Edmund Optics) equally divides the laser beam onto the two optical paths containing the sample and the reference cuvettes. Variations of the laser beam intensities passing through each one of the two cuvettes are measured by using two Si Photodiode (DET10A2 Photodiode by Thorlabs) that are indicated in Fig. 1 as PDS and PDR for the sample and reference optical channels, respectively. The PDS and PDR generated voltage pulses are the input signals of the tunable-gain, dual-channel, dual-phase LIA whose outputs are digitalized by a data acquisition board (DAQ) and sent to a PC for the measurement acquisitions in LabVIEW environment. Moreover, the LIA gain tuning is performed through the control voltage  $V_{CTRL}$  suitably provided by the DAQ board. Panel (a) of Fig. 2 shows the LTS experimental set-up mounted on a honeycomb optical breadboard. The 1 cm optical path UV fused quartz cuvettes used in the sample and reference optical channels are shown in panel (b). The cuvettes have a nominal optical transmittance close to 0.9 within the experimental laser tuning range. Panel (c) of Fig. 2 shows the fabricated prototype of the LIA with off-the-shelf components.

As mentioned in the previous paragraph, the standard measurement procedure for LTS is based on the double ratio method [19]. Referring to Fig. 1, the use of this method implies that the characterization of the nanoparticles contained in SC (i.e., the determination of their size and concentration) is achieved by performing two distinct LTS measurements: in the first one the cuvette positions are, for example, as shown in Fig. 1. The resulting transmission coefficient is  $T_1(\lambda, r) = S_1(\lambda, r)/R_1(\lambda)$  where, as before defined,  $\lambda$  and  $r$  are the laser wavelength and the radius of the nanoparticles, respectively. Here,  $S_1(\lambda, r)$  is the PDS voltage signal proportional to the laser beam intensity passing through the sample channel and  $R_1(\lambda)$  the PDR voltage signal proportional to the laser beam intensity passing through the reference channel that is independent from  $r$  since it contains only the liquid solution. For the second LTS measurement, the position of SC and RC in the optical channels are interchanged so obtaining a second transmission coefficient  $T_2(\lambda, r) = S_2(\lambda)/R_2(\lambda, r)$ . In this case,  $S_2(\lambda)$  is the PDS voltage signal proportional to the laser beam intensity passing through the sample channel that contains now the RC cuvette and  $R_2(\lambda, r)$  is the PDR voltage signal proportional to the laser beam intensity passing through the reference channel that contains now the SC cuvette. In this way, the procedure cancels out any difference in the two optical paths but at the expense to double the measurement time. The final result of these two LTS measurements is the transmission coefficient related to the presence of the particles in SC that is obtained by the ratio between the two transmission coefficients  $T_1(\lambda, r)$  and  $T_2(\lambda, r)$ :

$$T(\lambda, r) = \sqrt{\frac{T_1(\lambda, r)}{T_2(\lambda, r)}} = \sqrt{\frac{S_1(\lambda, r) R_2(\lambda, r)}{R_1(\lambda) S_2(\lambda)}} \quad (2)$$

This result makes clear that, even if the double ratio method does not need an initial calibration procedure of the LTS setup, a larger value of the measurement propagation of uncertainty is expected for  $T(\lambda, r)$  if compared to that one of a single ratio  $S(\lambda, r)/R(\lambda)$ . To overcome this problem that can strongly limit the LTS measurement sensitivity and resolution, we demonstrate that it is possible to perform the characterization of the nanoparticle contained in SC by a single LTS measurement after a proper calibration of the experimental apparatus. By acting on the gain of each one of the two channels of the LIA, the sample and reference signals are balanced for each wavelength by using the liquid solution inside both the SC and RC cuvettes (i.e., a blank sample in the two cuvettes). This method considerably reduces the total measurement time and increases the detection sensitivity and resolution of the apparatus. To illustrate in detail the method used for the LTS calibration, we refer to Fig. 3. As before outlined, in the first step (see panel (a)) both the sample SC and reference RC cuvettes are filled with the aqueous suspending medium (i.e., without the suspended particles) and, for every wavelength of the probing laser beam, the LIA gains  $G_1(\lambda)$  and  $G_2(\lambda)$  of each one of the two LIA input channels are varied until the ratio of the LIA output voltages  $S(\lambda)/R(\lambda)$  is equal to 1 within a value of the standard deviation of 0.5%.

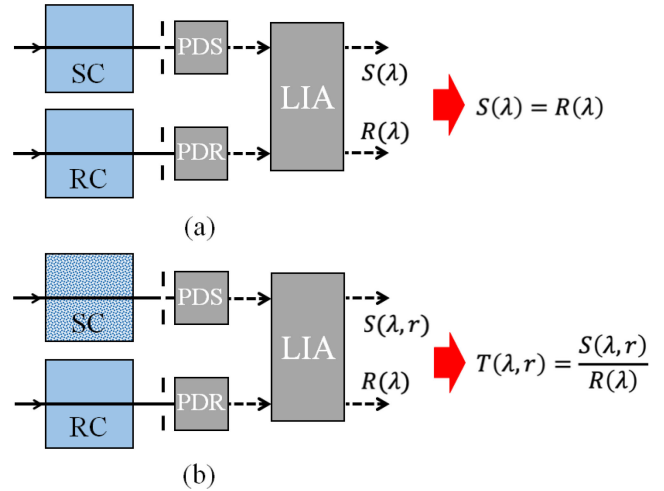


Fig. 3. Panel: (a) the experimental conditions used for the calibration of the signal  $S(\lambda)$  and the reference  $R(\lambda)$  amplitudes by varying the gain of each channel of the LIA; (b) the experimental conditions used for the LTS measurements of the sample transmission coefficient  $T(\lambda, r)$ : in this last case the sample cuvette SC contains the suspension of nanoparticles and the signal depends also on their radius.

This operation compensates the differences that may occur in the signal and reference optical paths and avoids the interchanging of the SC and RC cuvettes that may cause unpredictable optical misalignments. The achieved values of the gains  $G_1(\lambda)$  and  $G_2(\lambda)$  are automatically saved to be used for the LTS measurements. Thus, the SC cuvette can now be filled with the sample under investigation, i.e., the particle suspension (see panel (b) of Fig. 3) and the related transmission coefficients  $T(\lambda, r)$  are determined as the ratio between the measured signal  $S(\lambda, r)$  and reference  $R(\lambda)$ , setting for each wavelength the values of  $G_1(\lambda)$  and  $G_2(\lambda)$  previously determined in the calibration procedure.

### B. The Tunable-Gain Dual-Channel Dual-Phase Lock-In Amplifier (LIA)

The measurements of the amplitude variations of the voltage pulsed signals generated by the PDS and PDR photodiodes in the LTS experiments have been performed by using an *ad-hoc* tunable-gain, dual-channel, dual-phase LIA whose overall block scheme is shown in Fig. 4. Considering the laser source characteristics used for the experiments (see Fig. 1), the LIA internal blocks have been suitably designed and optimized in terms of the detection sensitivity and resolution, considering 5 ns pulsed voltage input signals at a repetition rate  $f_0 = 10$  Hz with a mean value different from zero. In this sense, referring to Fig. 4, all the filters, triggers, phase-shifters and amplifiers (i.e., the main stages/blocks composing the LIA) have been suitably implemented by using standard circuit topologies and configurations [46]. On the contrary, the LIA mixers and square root operations have been obtained by employing commercial active devices, as described in the following.

More in detail, at each one of the LIA input stages (i.e., for the *Input S* and *Input R* pulsed signals) the first block is

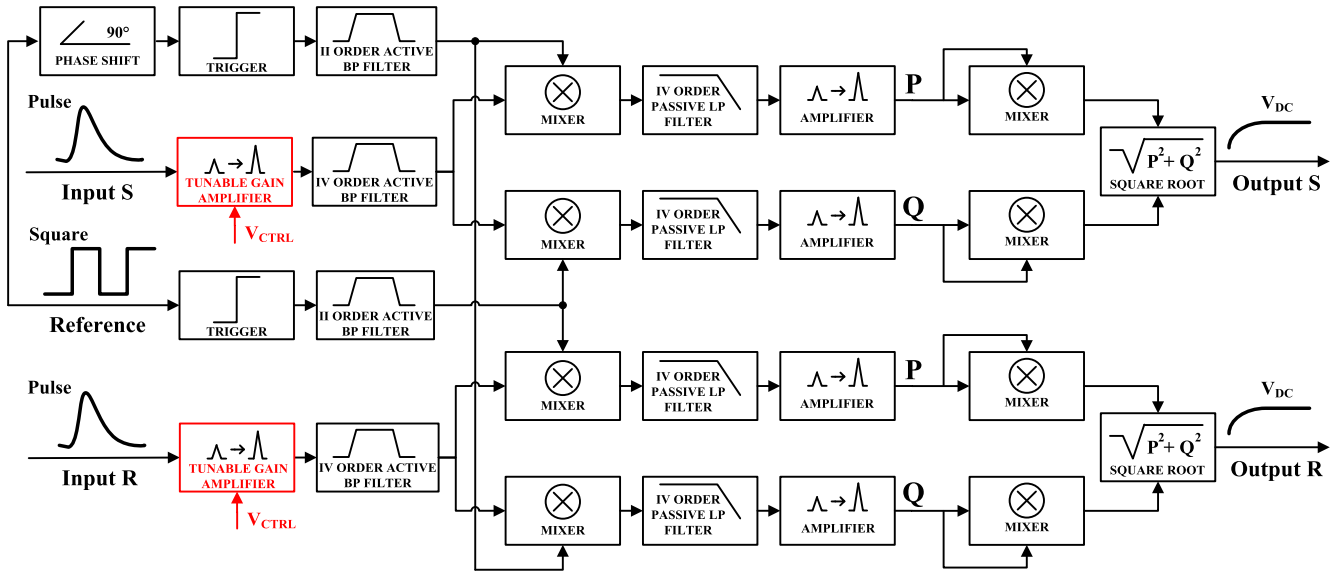


Fig. 4. Implemented block scheme of the proposed tunable-gain dual-channel dual-phase LIA.

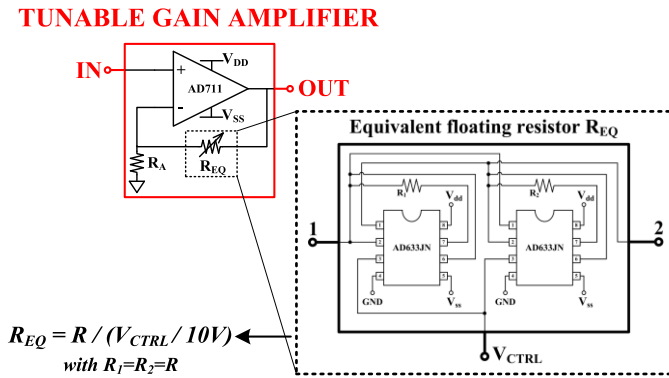


Fig. 5. Schematic circuit of the tunable gain amplifier and the voltage controlled floating resistor  $R_{EQ}$ .

a tunable gain amplifier based on an Operational Amplifier (OA) operating in a non-inverting configuration, as shown in the schematic circuit reported in Fig. 5, with a GBW = 3 MHz. It provides a variable gain, ranging from 2 up to 271, achieved by changing the value of the equivalent floating resistor  $R_{EQ}$  that is a tunable voltage-controlled device. This circuit topology has been implemented by two resistors and two AD633 analog multipliers (by Analog Devices) employed in a double-feedback configuration, as reported and described in [47]. It is capable to emulate a floating resistor having an overall equivalent resistance valued according to the non-linear relationship reported in the same Fig. 5. The gain tuning is performed by properly acting on the control voltage  $V_{CTRL}$ , through LabVIEW environment and the DAQ board, that suitably regulates the  $R_{EQ}$  value. The tunable gain amplifier is combined with the fourth-order active band-pass filter employed in order to: i) reduce the harmonic content of the input signal and the associated noise bandwidth; ii) eliminate the input disturbs and/or interferences; iii) achieve and

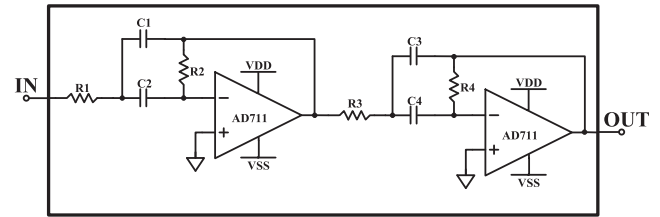


Fig. 6. Schematic circuit of the fourth-order active band-pass filter.

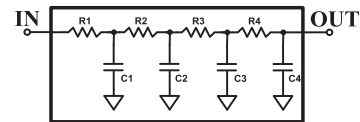


Fig. 7. Schematic circuit of the fourth-order passive low-pass filter.

amplify the main harmonic components of the input signals. The schematic circuit of this stage is reported in Fig. 6. It has been implemented by a cascade of two active second-order multiple negative feedback inverting filter topology centered at  $f_0 = 10$  Hz with a maximum gain of about 550 and a quality factor  $Q = 12.5$  corresponding to a bandwidth  $BW = 0.8$  Hz. Then, after the demodulation stage (i.e., the mixer block), the fourth-order passive low-pass filter allows to extract the DC component of the resulting signal and, at the same time, to regulate the overall system response time. This filter is based on a simple passive topology composed by a cascade of four RC-cells, as shown in Fig. 7, with a maximum gain of about 0.98 and a resulting cut-off frequency  $f_t \approx 10$  mHz, much smaller than  $f_0 = 10$  Hz (i.e., the LIA reference operating frequency that corresponds to the laser repetition rate  $f_0$ ) and its main harmonics. Moreover, an additional amplifier has been also included to further increase the instrument total gain and to enhance the LIA detection

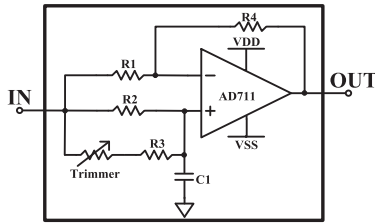


Fig. 8. Schematic circuit of the phase shifter block.

sensitivity and resolution. This stage makes use of an OA in a non-inverting configuration with a fixed gain equal to 10 and a  $GBW = 3$  MHz. Finally, the resulting Phase ( $P$ ) and Quadrature ( $Q$ ) signals are squared through further mixer blocks and, by means of a square root operation of the sum  $P^2 + Q^2$ , the final  $V_{DC}$  output signal, proportional to the amplitude of the input pulses, is provided. Referring to the square wave reference signal, a phase shifter block has been included so to add a  $90^\circ$  phase shift, at the reference frequency  $f_0 = 10$  Hz and with a unitary gain, between the  $P$  and  $Q$  paths. The schematic circuit implementation, including a trimmer for a phase shift fine tuning, is reported in Fig. 8. In addition, trigger blocks are also employed, implemented through OAs in an open-loop comparator configuration, so to provide square wave signals with fixed and constant values (i.e., low level =  $V_{SS}$ , high level =  $V_{DD}$ ). Finally, a second-order active band-pass filter has been included to extract the main harmonic component of the reference signal employed for the demodulation operation. It has been implemented by an active second-order multiple negative feedback inverting filter topology ( $f_0 = 10$  Hz, maximum gain = 22 and quality factor  $Q = 5$  corresponding to a bandwidth  $BW = 2$  Hz; see the first block of the schematic circuit reported in Fig. 6).

A LIA prototype has been fabricated on a PCB through commercial discrete components and devices (see Fig. 2). In particular, all the passive elements are accurate passive components, with 1% tolerance, whose values have been evaluated through laboratory measurement equipments/instrumentations (e.g., high-accuracy high-precision impedance-meters). In this regard, all the values of the main parameters, characteristics and specifications of the LIA here reported are experimentally measured (and not theoretically determined). All the experimental measurements have been done at room temperature. Moreover, all the components implementing the main LIA active blocks are AD711 BiFET high speed OA (by Analog Devices). The mixers and the  $R_{EQ}$  employ AD633 analog multipliers (by Analog Devices) and the square root stage uses the AD734 high speed four-quadrant analog multiplier (by Analog Devices). All the LIA active components are powered at a DC dual supply voltage equal to  $\pm 15$  V and the resulting total power consumption of the LIA prototype is about 3.5 W (corresponding to a current dissipation of about 230 mA).

Preliminary electrical validations and experimental characterizations of the developed LIA prototype have been conducted by performing time-domain measurements and analyzing the input-output voltage signals. In particular, Fig. 9 shows the

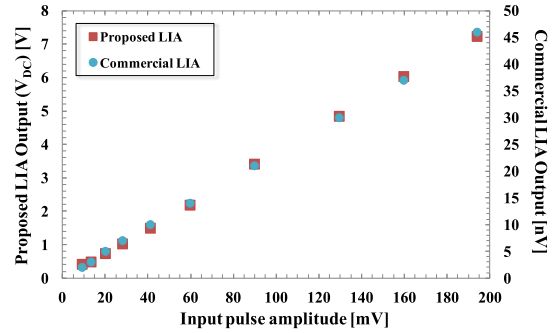


Fig. 9. LIA experimental characterization: measurement results of the proposed LIA output (for a fixed overall gain of about 123 dB) compared with those ones performed with a commercial LIA as a function of the amplitude of the input pulsed signal ranging from 10 mV to 195 mV.

results related to the measured  $V_{DC}$  output signal of the LIA (i.e., Output S) as a function of the amplitude change of an input pulsed signal (i.e., Input S) electrically provide by a laboratory signal generator (PHILIPS PM 5705) with the following characteristics:  $f_0 = 10$  Hz; 5 ns pulse width; variable pulse amplitude ranging from 10 mV to 195 mV (a square wave reference signal has been also provided by the same instrument). As reported in Fig. 9, the achieved sensitivity of the proposed LIA is about 37.5 [V/V], setting a LIA total voltage gain to about 123 dB achieved through the contributions of all the main blocks of the LIA. Since the measured maximum output noise rms level is about 2 mV, a minimum detection resolution of about  $53 \mu\text{V}$  can be achieved (calculated as the ratio between the LIA output noise level and its sensitivity). This noise level can be considered the overall residual LIA output noise mainly due to the following two contributions (i.e., equivalent noise sources): the input noise combined with the input and the reference signals at the LIA inputs; the intrinsic noise level coming from the overall circuitry (i.e., from the active electronic components/devices and from the passive elements employed in the prototype PCB). Moreover, for a comparative analysis, measurement results achieved by using a commercial LIA (SRS830DSP digital LIA by Stanford Research Systems), at the same operating conditions reported above, are also shown in Fig. 9 demonstrating a resulting sensitivity of about  $0.234 \times 10^{-6}$  [V/V]. In this case, the evaluated maximum output noise level is lower than 0.1 nV so achieving a minimum detection resolution of about  $427 \mu\text{V}$ . Finally, the measured outputs, corresponding to the specific amplitudes of the pulsed input signal, ranges from 2 nV to 46 nV with the commercial LIA while the proposed LIA is capable to provide an output signal amplitude ranging from 0.41 V up to 7.23 V. This demonstrates that the detection sensitivity enhancement introduced by the developed LIA, with respect to a commercial/standard solution, is equal to about  $160 \times 10^6$ , while the minimum detection resolution has been improved of about a factor 8 (i.e.,  $427 \mu\text{V}/53 \mu\text{V}$ ).

### III. EXPERIMENTAL MEASUREMENTS: DATA AND RESULTS

The experimental validation of the proposed variable gain calibration method has been first performed by LTS

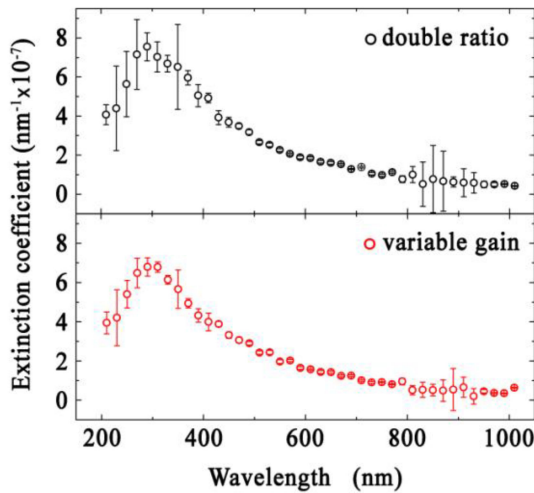


Fig. 10. The extinction coefficient of a suspension of NIST standard nanoparticles with a nominal size and concentration equal to  $2r = 508$  nm and  $1.0 \times 10^9$  particles/ml by using the double ratio method (upper panel), and the variable gain calibration procedure (lower panel).

measurements of the size and concentration of a suspension of NIST standard polystyrene nanoparticles (Duke Standard by Thermo Scientific - Waltham, MA - USA). The spherical nanoparticle nominal average radius and concentration were equal to  $r = 254 \pm 4$  nm and  $C = 1.0 \times 10^9$  particles/ml, respectively. In Fig. 10 are reported the LTS measurement of the extinction coefficients by using the double ratio method (upper panel), and the variable gain calibration procedure (lower panel). In particular, the LTS measurement with the double ratio method has been performed by using the dual-channel LIA by setting the same constant gain equal to 10. This choice fulfills both the conditions to use a laser intensity for the entire measurement wavelength range well below the Si photodiode saturation value and to maximize the overall signal-to-noise ratio. Furthermore, we point out that the experimental uncertainties (i.e., the error bars) associated to the extinction coefficient data of Fig. 10 (and later on for the data of Fig. 12 and Fig. 13) have been calculated by the standard statistical method of the propagation of uncertainty [48]. This was done by inserting (2) into (1) for the double ratio method and  $T(\lambda, r) = S(\lambda, r)/R(\lambda)$  in (1) for the variable gain procedure. As a first qualitative remark, the error bars associated to the experimental data are significantly smaller for the variable gain calibration procedure. This observation is quantitative supported by the results of Fig. 11 that reports the density distributions as a function of the particle radius, as obtained by using the inverting square root-based algorithm applied to the extinction data of Fig. 10. The data shown in Fig. 11 have been taken by varying the wavelength of the probing laser beam passing through the SC and RC cuvettes in steps of 10 nm. By considering the fourth-order passive low-pass filter used in the LIA channels architecture having a cut-off frequency  $f_t \approx 10$  mHz, for each wavelength step, the average value of the laser intensities passing through the SC and RC cuvettes and the relative experimental uncertainties have been calculated by waiting 3 LIA time constants equal to about

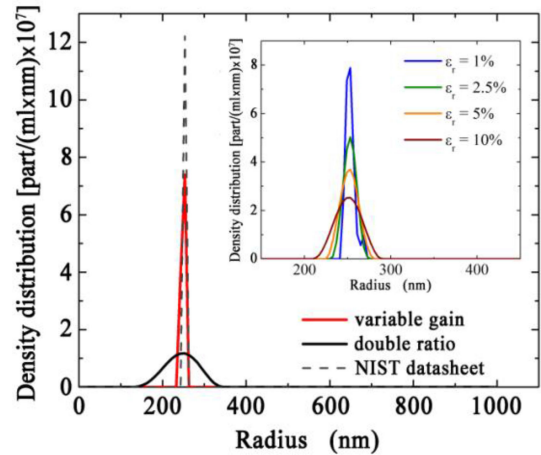


Fig. 11. Density distribution as a function of the radius of a suspension of NIST standard polystyrene nanoparticles achieved by performing LTS measurements using the double ratio method (black curve) and the variable gain calibration procedure (red curve). In the inset the results of the numerical simulations demonstrating the effects of the decrease of the extinction relative errors on the average value and standard deviation of the nanoparticle density distribution.

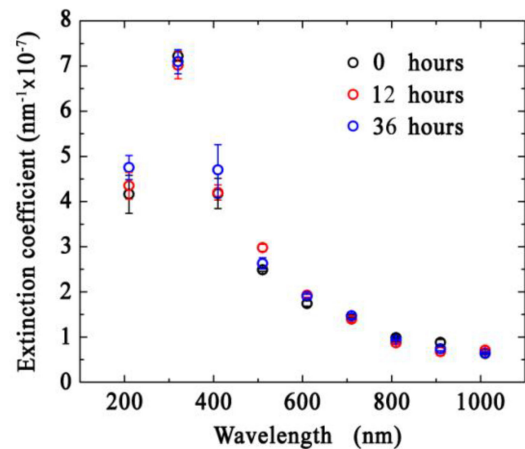


Fig. 12. The extinction coefficient of a suspension of NIST standard nanoparticles with a nominal size and concentration equal to  $2r = 508$  nm and  $1.0 \times 10^9$  particles/ml by performing LTS measurements after 12- and 36-hours respect to the variable gain calibration procedure.

50 s before acquiring the dual-channel LIA output amplitudes of 100 laser shots. At present, these experimental conditions represent the best compromise between the need to determine with high accuracy the average size and density distributions of the nanoparticles, and the total LTS measurement time corresponding to 90 minutes.

Referring to Fig. 11, the calculated particle average radius and concentrations (distribution integral) are equal to  $r_{DR} = (227 \pm 50)$  nm and  $C_{DR} = (1.29 \pm 0.07) \times 10^9$  particles/ml for the double ratio method and  $r_{VG} = (250 \pm 6)$  nm and  $C_{VG} = (1.14 \pm 0.06) \times 10^9$  particles/ml for the variable gain calibration procedure. The fractional uncertainties associated to the measured particle radius are equal to  $\varepsilon(r_{DR}) = 22\%$  and  $\varepsilon(r_{VG}) = 2.4\%$  for the double ratio method and the variable gain calibration procedure, respectively. Thus, the variable gain

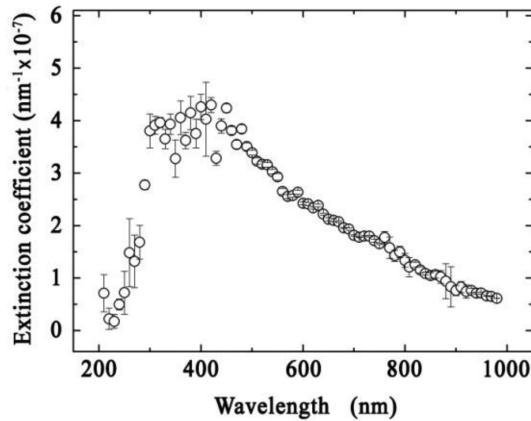


Fig. 13. Extinction coefficient as a function of the laser wavelength of orange juice extracellular vesicles suspended in PBS buffer measured after the LTS calibration procedure.

calibration procedure decreases the fractional uncertainty of a value close to one order of magnitude. This result is further confirmed if we compare the achieved particle radius with the nominal one: the relative deviations from the nominal particle radius,  $r$ , are equal to  $\Delta(r_{DR}) = [r - r_{DR}]/r = 10.6\%$  and  $\Delta(r_{VG}) = [r - r_{VG}]/r = 1.6\%$  for the double ratio method and the variable gain calibration procedure, respectively.

In order to analyze the effects of the decrease of the relative errors of the experimental data on the determination of the particle size and density, we performed a series of numerical simulations assuming that the NIST nanoparticle size around the datasheet nominal value are statistically dispersed following a Gaussian distribution. We calculated the expected extinction coefficients from the Mie theory associating different fractional uncertainties in their determination ranging from  $\epsilon_r = 1\%$  to  $\epsilon_r = 10\%$ . By using the Tikhonov inversion method, the achieved results of the simulations, reported in the inset of Fig. 11, demonstrate that the particle size distribution mean value results unaltered and the only effect of the decrease of the relative error associated to the experimental data is the decrease of the value of the particle size and density distribution standard deviation.

Differently from the results obtained for the particle radius, the results achieved for the particle concentration by using the double ratio method and the variable gain calibration are quite similar in terms of the fractional uncertainties. From the LTS measurements, in fact, we found that indetermination on the concentrations are  $\epsilon(C_{DR}) = 5.4\%$  and  $\epsilon(C_{VG}) = 5.3\%$  for the double ratio and variable gain calibration procedure. On the other hand, the variations respect to the nominal particle concentration are equal to  $\Delta(C_{DR}) = 29\%$  and  $\Delta(C_{VG}) = 14\%$  with an improvement of a factor 2 obtained when the variable gain calibration procedure is employed. From the above results, we can conclude that the proposed variable gain calibration procedure is capable to strongly increase the resolution in determining the average particle size respect to the results achievable by using the double ratio procedure. For what concerns the determination of the particle concentration, both the methodology gives values close to the nominal one even if the variable gain procedure

demonstrates to be able to decrease of a factor 2 the variation between the measured and nominal values. This result is not surprising since, as shown in Fig. 11, the distribution integral does not depend on the size resolution achieved in the LTS measurement for the variation of 10 nm of the probing laser wavelength. In other words, under the same experimental conditions, the double ratio method and the variable gain calibration procedure are both capable to identify the particles (even if with a different size resolution) in such a way to give very close values on their concentration. The next important step to further validate the variable gain calibration procedure is to prove the robustness and reliability features of this method to give the same results on the particle size and concentration even long time after the calibration procedure ended.

For this purpose, the LTS measurement of the extinction coefficient of the NIST standard nanoparticles of Fig. 10(lower panel) has been repeated 12 and 36 hours later the variable gain calibration procedure by using the same values of  $G_1(\lambda)$  and  $G_2(\lambda)$  there determined. The results are shown in Fig. 12. Respect to Fig. 10, this Figure reports for clarity, only a limited number of experimental data. The full analysis of the achieved extinction curves allows to calculate the particle average radius and concentration:  $r_{VG}(12h) = (249 \pm 7)$  nm and  $C_{VG}(12h) = (1.19 \pm 0.06) \times 10^9$  particles/ml after 12 hours;  $r_{VG}(36h) = (247 \pm 10)$  nm and  $C_{VG}(36h) = (1.12 \pm 0.05) \times 10^9$  particles/ml after 36 hours. The comparison of these results with those ones obtained just after the variable gain procedure, demonstrates that the determination of the nanoparticle size and concentration remains well within the experimental uncertainty. In particular, only a slight increase from 2.4% to 4.0% of the relative error in the value of particle radius has been observed, while remains constant those ones of the particle concentrations.

After these experimental analyzes devoted to validate the LTS apparatus employing the variable gain calibration procedure, we proceeded to measure the size and concentration of biological nanostructures. For this purpose, we characterized extracellular vesicles extracted from 175 ml of orange juice by centrifugation followed by filtration. The so obtained sample was resuspended in 1 ml of Phosphate Buffer Saline (PBS) medium, which was also used as the reference. A preliminary characterization of this sample has been performed by using the Dynamic Light Scattering (DLS) technique. The resulting DLS intensity weighted distribution obtained by employing a MALVERN NanoZetasizer apparatus (Malvern Instruments LTD, Worcestershire, U.K.) has shown the presence of two populations of vesicles with a radius of  $(25 \pm 5)$  nm and  $(372 \pm 90)$  nm. Fig. 13 shows the extinction coefficient of the same sample of extracellular vesicles suspension obtained from the LTS measurements after performing the variable gain calibration procedure with only the PBS buffer filling both the SC and RC cuvettes to determine the values of the gains  $G_1(\lambda)$  and  $G_2(\lambda)$ . The dependence of the extinction coefficient on the laser wavelength is that one expected for nanostructures of nanometer size and presents a maximum at a wavelength equal to about 400 nm. Proceeding as before, the extinction coefficient data were analyzed by means of a square root-based algorithm to determine the density distribution as

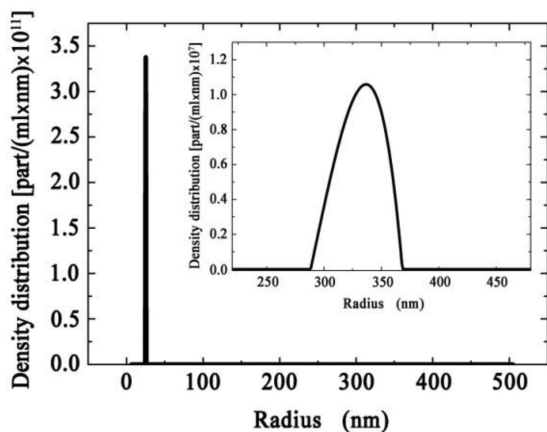


Fig. 14. Density distribution as a function of the radius of the orange juice extracellular vesicles. In the inset is highlighted the peak at higher radius due to the presence of aggregates of vesicles that results to be more than 3 order of magnitude lower than the peak of the single vesicles.

a function of the vesicle radius. The result of the analysis is reported in Fig. 14. The density distribution presents two peaks: the first one is located for a value of the radius of the extracellular vesicles equal to  $(25 \pm 2)$  nm; the second one, much broader, is related to particles with a radius of  $(340 \pm 50)$  nm and is reported in the inset of Fig. 14 with the vertical axis decreased of 3 orders of magnitude.

This last density distribution peak comes from aggregations of different numbers of vesicles. As a final remark, we found that the vesicle density distribution populations are in good agreement with those ones achieved by the DLS measurements. However, it should be noted that the slightly different radius measured for the vesicle population having the higher average size (if compared with the value obtained by the LTS measurements) can be ascribed to the fact that the DLS intensity distribution depends on the sixth power of the particle radius, with a consequent overestimation for the bigger particle sizes. A simple integration gives the absolute concentration of the two species of particles in the suspension:  $(3.5 \pm 0.2) \times 10^{11}$  particles/ml for the single vesicles and  $(5.4 \pm 0.3) \times 10^8$  particles/ml for the aggregates. It is worth noting from these results that a single LTS measurement allows to determine the size and the concentration of different vesicles populations even if their values differ of orders of magnitude. These results obtained for a sample of orange juice extracellular vesicles are very encouraging since they demonstrate the possibility to systematically use the variable gain calibration method for the LTS determination of the size and concentration of poly-monomodal distribution of nanoparticles, like the investigated vesicles, but also of bacteria (i.e., particles bigger than vesicles) particularly important in the food and biomedical industry.

#### IV. CONCLUSION

This paper reported on a novel variable gain calibration procedure for instruments performing laser transmission spectroscopy capable to determine by a single measurement, the size and

concentration of mono- and poly-dispersed nanoparticles. The proposed calibration procedure is based on the use of an ad hoc designed and fabricated tunable-gain, dual-channel dual-phase lock-in amplifier whose electronic solutions and circuitries are reported in detail. Respect to the standard double ratio method that needs two different LTS measurements for the determination of the size and concentration of nanoparticles, the variable gain calibration procedure allows to decrease of an order of magnitude the experimental indetermination of the particle size by performing a single LTS measurement. In the paper, this achievement is demonstrated by measuring size and density distribution of a suspension of NIST standard polystyrene nanoparticles. Moreover, the robustness and reliability of the proposed methodology has been tested by repeating the LTS measurements on the same samples 12 and 36 hours after the variable gain procedure was firstly accomplished. In particular, only a slight increase from 2.4% to 4.0% of the fractional uncertainty in the value of particle radius has been observed, remaining constant that one of the particle concentration. As a case example of biological applications, we performed LTS measurements of the size and density distributions of a population of monodispersed extracellular vesicles extracted from orange juice with the presence of their aggregates having a size larger than a factor 14 (i.e., 25 nm for single vesicles, and 340 nm for the aggregates) and a concentration smaller than 3 orders of magnitude. These results are of particular interest for future characterization of bacteria (bigger than vesicles) that are important for a wide range of biomedical applications as well as for industrial food preparation and conservation.

#### REFERENCES

- [1] R. J. Simpson, J. W. Lim, R. L. Moritz, and S. Mathivanan, "Exosomes: Proteomic insights and diagnostic potential," *Expert Rev. Proteomics*, vol. 6, no. 3, pp. 267–283, 2009.
- [2] O. M. Elsharkasy *et al.*, "Extracellular vesicles as drug delivery systems: Why and how?," *Adv. Drug Del. Rev.*, vol. 159, pp. 332–343, 2020.
- [3] İ. Eroğlu and M. İbrahim, "Liposome–ligand conjugates: A review on the current state of art," *J. Drug Targeting*, vol. 28, no. 3, pp. 225–244, 2020.
- [4] P. da Silva Malheiros, Y. M. S. Micheletto, N. P. da Silveira, and A. Brandelli, "Development and characterization of phosphatidylcholine nanovesicles containing the antimicrobial peptide nisin," *Food Res. Int.*, vol. 43, no. 4, pp. 1198–1203, 2010.
- [5] A. Popat *et al.*, "Adsorption and release of biocides with mesoporous silica nanoparticles," *Nanoscale*, vol. 4, no. 3, pp. 970–975, 2012.
- [6] A. L. Leitão and F. J. Enguita (ed.s.), *Non-coding RNAs and Inter-Kingdom Communication*. Berlin, Germany: Springer International Publishing, 2016.
- [7] B. L. Deatherage and B. T. Cookson, "Membrane vesicle release in bacteria, eukaryotes, and archaea: A conserved yet underappreciated aspect of microbial life," *Infection Immun.*, vol. 80, no. 6, pp. 1948–1957, 2012.
- [8] C. Begly, D. Ackart, J. Mylius, R. Basaraba, A. J. Chicco, and T. W. Chen, "Study of real-time spatial and temporal behavior of bacterial biofilms using 2-D impedance spectroscopy," *IEEE Trans. Biomed. Circuit, Syst.*, vol. 14, no. 5, pp. 1051–1064, Oct. 2020.
- [9] D. D. Taylor and C. Gerceel-Taylor, "MicroRNA signatures of tumor-derived exosomes as diagnostic biomarkers of ovarian cancer," *Gynecologic Oncol.*, vol. 110, no. 1, pp. 13–21, 2008.
- [10] W. Zhang, X. Zhou, H. Zhang, Q. Yao, Y. Liu, and Z. Dong, "Extracellular vesicles in diagnosis and therapy of kidney diseases," *Amer. J. Physiol.-Renal Physiol.*, vol. 311, no. 5, pp. F844–F851, 2016.
- [11] U. M. Pal *et al.*, "Towards a portable platform integrated with multispectral noncontact probes for delineating normal and breast cancer tissue based on near-infrared spectroscopy," *IEEE Trans. Biomed. Circuit, Syst.*, vol. 14, no. 4, pp. 879–888, Aug. 2020.

- [12] J. Bai *et al.*, "Extraction of DNA from orange juice, and detection of bacterium candidatus liberibacter asiaticus by real-time PCR," *J. Agricultural food Chem.*, vol. 61, no. 39, pp. 9339–9346, 2013.
- [13] B. K. Mitall and S. K. Garg, "Anticarcinogenic, hypocholesterolemic, and antagonistic activities of lactobacillus acidophilus," *Crit. Rev. Microbiol.*, vol. 21, no. 3, pp. 175–214, 1995.
- [14] N. P. Shah, W. K. Ding, M. J. Fallourd, and G. Leyer, "Improving the stability of probiotic bacteria in model fruit juices using vitamins and antioxidants," *J. Food Sci.*, vol. 75, no. 5, pp. 278–282, 2010.
- [15] J. Mu *et al.*, "Interspecies communication between plant and mouse gut host cells through edible plant derived exosome-like nanoparticles," *Mol. Nutr. Food Res.*, vol. 58, 2014, Art. no. 15611573.
- [16] M. Zhang, E. Viennois, C. Xu, and D. Merlin, "Plant derived edible nanoparticles as a new therapeutic approach against diseases," *Tissue Barriers*, vol. 4, 2016, Art. no. e1134415.
- [17] M. De Robertis *et al.*, "Blueberry-derived exosome-like nanoparticles counter the response to TNF- $\alpha$ -Induced change on gene expression in EA. hy926 cells," *Biomolecules*, vol. 10, no. 742, pp. 1–17, 2020.
- [18] H. Kang, J. Kim, and J. Park, "Methods to isolate extracellular vesicles for diagnosis," *Micro Nano Syst. Lett.*, vol. 5, no. 5, no. 15, pp. 1–11, 2017.
- [19] F. Li, R. Schafer, C. T. Hwang, C. E. Tanner, and S. T. Ruggiero, "High-precision sizing of nanoparticles by laser transmission spectroscopy," *Appl. Opt.*, vol. 49, no. 34, pp. 6602–6611, 2010.
- [20] S. P. Egan *et al.*, "Rapid molecular detection of invasive species in ballast and harbor water by integrating environmental DNA and light transmission spectroscopy," *Environ. Sci. Technol.*, vol. 49, pp. 4113–4121, 2015.
- [21] J. M. Marr *et al.*, "The role of lateral tension in calcium-induced DPPS vesicle rupture," *Langmuir*, vol. 28, pp. 11874–11880, 2012.
- [22] F. Li *et al.*, "Quantitative and rapid DNA detection by laser transmission spectroscopy," *PLoS One*, vol. 6, no. 12, 2011, Art. no. e29224.
- [23] B. J. Berne and R. Pecora, *Dynamic Light Scattering: With Applications to Chemistry, Biology, and Physics*. Chelmsford, MA, USA: Courier Corporation, 2000.
- [24] A. Grimaldi *et al.*, "Microglia-derived microvesicles affect microglia phenotype in glioma," *Front. Cellular Neurosci.*, vol. 13, no. 41, pp. 1–14, 2019.
- [25] *Lock-in Amplifiers and Pre-Amplifiers*. Princeton Appl. Res. Corp., 1971.
- [26] M. L. Meade, *Lock-in Amplifiers: Principles and Applications*. London: Peter Peregrinus Ed., 1983.
- [27] M. Davidovic, J. Seiter, M. Hofbauer, W. Gaberl, and H. Zimmermann, "Monolithically integrated dual-lock-in optical sensor," *IET Electron. Lett.*, vol. 50, pp. 306–308, 2014.
- [28] F. Paz and M. Ordóñez, "High-performance solar MPPT using switching ripple identification based on a LIA," *IEEE Trans. Ind. Electron.*, vol. 63, no. 6, pp. 3595–3604, Jun. 2016.
- [29] S. Sutula, C. Ferrer, and F. Serra-Graells, "A 4000 $^{\circ}$ W Hz-range lock-in A/D frontend channel for infrared spectroscopic gas recognition," *IEEE Trans. Circuit, Syst. I*, vol. 58, pp. 1561–1568, 2011.
- [30] A. De Marcellis, E. Palange, N. Liberatore, and S. Mengali, "Low-cost portable 1 MHz lock-in amplifier for fast measurements of pulsed signals in sensing applications," *IEEE Sensors Lett.*, vol. 1, no. 4, pp. 1–4, 2017.
- [31] G. Gervasoni *et al.*, "A 12-channel dual-lock-in platform for magneto-resistive DNA detection with PPM resolution," in *Proc. IEEE Biomed. Circuits Syst. Conf.*, Dec. 2014, pp. 316–319.
- [32] D. Palomeque-Mangut, J. L. Auñs, and F. Duque-Carrillo, "Comparative study of CMOS lock-in amplifiers for wideband bioelectrical impedance measurements," in *Proc. IEEE Int. Conf. Electron., Circuits Syst.*, 2017, pp. 416–419.
- [33] M. Noormohammadi Khiarak, S. Martel, and B. Gosselin, "CMOS optoelectronic Lock-in amplifier with semi-digital automatic phase alignment," in *Proc. IEEE Int. Symp. Circuits Syst.*, 2019, pp. 1–5.
- [34] A. M. Chiarelli *et al.*, "Wearable, fiber-less, multi-channel system for continuous wave functional near infrared spectroscopy based on silicon photomultipliers detectors and lock-in amplification," in *Proc. IEEE Annu. Int. Conf. Eng. Med. Biol. Soc.*, 2019, pp. 60–66.
- [35] R. S. Da Fonseca, M. J. C. Bonfim, R. D. Gonçalves, R. Da Silva Ferraz, and E. Parente Ribeiro, "Water pollution assessment by microcontroller-based lock-in amplifier," in *Proc. IEEE Int. Symp. Instrum. Syst., Circuits Transducers*, 2019, pp. 1–5.
- [36] A. De Marcellis, G. Di Patrizio Stanchieri, M. Faccio, E. Palange, and T. G. Constantinou, "A 300 mbps 37 pJ/bit pulsed optical biotelemetry," *IEEE Trans. Biomed. Circuit, Syst.*, vol. 14, no. 3, pp. 441–451, Jun. 2020.
- [37] Q. Lin *et al.*, "A 119dB dynamic range charge counting light-to-digital converter for wearable PPG/NIRS monitoring applications," *IEEE Trans. Biomed., Circuit, Syst.*, vol. 14, no. 4, pp. 800–810, Aug. 2020.
- [38] F. Marefat, R. Erfani, K. L. Kilgore, and P. Mohseni, "A 280  $\mu$ W 108 dB DR PPG-Readout IC with reconfigurable 2nd-order incremental  $\Delta\Sigma$ M front-end for direct light-to-digital conversion," *IEEE Trans. Biomed. Circuit, Syst.*, vol. 14, no. 6, pp. 1183–1194, Dec. 2020.
- [39] L. D. Quang *et al.*, "Biological living cell in-flow detection based on microfluidic chip and compact signal processing circuit," *IEEE Trans. Biomed., Circuit, Syst.*, vol. 14, no. 6, pp. 1371–1380, Dec. 2020.
- [40] A. De Marcellis *et al.*, "Balanced laser transmission spectroscopy based on a tunable gain double channel LIA for nanoparticles detection in biomedical applications," in *Proc. IEEE Biomed. Circuits Syst. Conf.*, Nara, Japan, 2019, pp. 1–4, doi: 10.1109/BIOCAS.2019.8918741.
- [41] J. Weese, "A reliable and fast method for the solution of fredhol integral equations of the first kind based on Tikhonov regularization," *Comput. Phys. Commun.*, vol. 69, no. 1, pp. 99–111, 1992.
- [42] W. J. Wiscombe, "Improved mie scattering algorithms," *Appl. Opt.*, vol. 19, no. 9, pp. 1505–1509, 1980.
- [43] C. F. Bohren and D. R. Huffman, *Absorption and Scattering of Light by Small Particles*. Hoboken, NJ, USA: Wiley, 2008.
- [44] N. Sultanova, S. Kasarova, and I. Nikolov, "Dispersion proper ties of optical polymers," *Acta Physica Polonica-Ser. A Gen. Phys.*, vol. 116, no. 4, pp. 585–587, 2009.
- [45] [Online]. Available: <https://refractiveindex.info>
- [46] B. Razavi, *Microelectronics*. Hoboken, NJ, USA: Wiley, 2014.
- [47] G. Q. Zhong, R. Bargar, and K. S. Halle, "Circuits for voltage tuning the parameters of chua's circuit: Experimental application for musical signal generation," *J. Franklin Inst.*, vol. 331, no. 6, pp. 743–784, 1994.
- [48] J. R. Taylor, *An Introduction to Error Analysis: The Study of Uncertainties in Physical Measurements*. Mill Valley, CA, USA: Univ. Science Books, 1997.



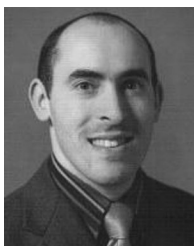
**Angelo Sarra** received the master's degree in physics from the Sapienza University, Rome, Italy, in 2016 and the Ph.D. degree in condensed matter physics, nanoscience and complex systems, from the University of Roma Tre, Rome, Italy, in 2020. He is currently a Research Fellow with the Institute of Complex Systems of the National Research Council, Rome, Italy. During his Ph.D., he realized the experimental apparatus and developed the data acquisition and analysis software to perform Laser Transmission Spectroscopy measurements. His main research interests

include the morphological characterization of colloidal systems, nanostructures, and biomaterials for drug delivery including lipid vesicles and thermo-responsive microgels.



**Guido Di Patrizio Stanchieri** received the master's degree (*cum laude*) in 2017 in electronic engineering from the University of L'Aquila, L'Aquila, Italy, where he is currently working toward the Ph.D. degree. Starting from 2016, he joined an External Scientific Collaboration with the Department of Industrial and Information Engineering and Economics, University of L'Aquila. His main research interests include the design and implementation of digital electronic circuits and systems for signal processing and data communication in biomedical, and robotics

integrated applications.



**Andrea De Marcellis** (Member, IEEE) received the degree in electronic engineering and the Ph.D. degree in microelectronics from the University of L'Aquila, L'Aquila, Italy, in 2005 and 2009, respectively. He is currently an Associate Professor of electronics with the Department of Industrial and Information Engineering and Economics, University of L'Aquila. His main research interests include the design of mixed-signal electronic and optoelectronic integrated circuits and systems for signal conditioning, data processing, optical sensing and communication links for biomedical applications. He has coauthored a book and two book-chapters in 2011, 2013, and 2020, respectively and more than 160 scientific publications in international journals and conference proceedings. He is the Chair of the Technical Committee "Optoelectronic sensing systems" of the IEEE Italy Sensors Chapter and is a Member of the Editorial Board of *Universal Journal of Electrical and Electronic Engineering*.



**Paolo Postorino** received the Ph.D. degree in condensed matter physics from the University of Perugia, Perugia, Italy and University of L'Aquila, L'Aquila, Italy. He is a Professor of condensed matter physics with the Physics Department of the Sapienza Università di Roma (The Sapienza University of Rome), Rome, Italy. Since 2000, he has been the Head of the High-Pressure Spectroscopy Research Group. He has authored or coauthored more than 160 papers. His research interests include the study of strongly correlated materials, including transition-metal oxides and high-T<sub>c</sub> superconductors, and low-dimensional materials such as single or few layer systems, nanotubes, nanowires, and plasmonic nanoparticles.



**Federico Bordi** received the degree in physics from the Sapienza University of Rome, Rome, Italy, in 1984 and the Diploma as Specialist in medical physics from the Tor Vergata University of Rome, Rome, Italy. Since 2002, he has been an Associate Professor of physics with the Department of Physics, Sapienza University of Rome. From 1988 to 1990, he was a Researcher with the Physics Laboratory, the Italian National Institute of Health, Rome, Italy and from 1990 to 2002 a Researcher with the Department of Internal Medicine of the Tor Vergata University. His research interests include aggregation dynamics in charged colloidal systems, self-assembly of oppositely charged colloids and polymers, self-assembly of supramolecular structures to be used as drug delivery and gene delivery nanovectors, transport properties and structure of biological cell membranes and model membranes, dielectric spectroscopy investigation of transmembrane electrical transport in biological cell and model membranes, electrical transport properties of polymer solutions and colloidal systems, effect of counterion condensation of chain conformation and polymer-solvent interactions on the electrical transport properties of polyelectrolyte solutions, and interaction between colloidal particles and charged or uncharged polymers.



**Elia Palange** received the Laurea degree in physics from the Sapienza University of Rome. He is currently an Associate Professor of physics and nanophotonic and the Supervisor of Electronic and Photonic Integrated Circuits and Systems Laboratory with the Department of Industrial and Information Engineering and Economics, University of L'Aquila, L'Aquila, Italy. His research interests include laser physics, the linear and nonlinear optical properties of bulk semiconductor and of nanometer-sized quantum semiconductor heterostructures, the design and implementation of novel photonics multifunctional devices, sensors based on the linear and nonlinear optical properties of metamaterials, and functionalized metasurfaces combined with high-sensitive optoelectronic detection systems.